IJMMM International Journal of Minerals, Metallurgy and Materials 矿物冶金与材料学报（英文版）

Comparison of the interface reaction behaviors of $CaO–V_2O_5$ and $MnO_2–V_2O_5$ solid-state systems based on the diffusion couple method

Jing Wen, Hongyan Sun, Tao Jiang, Bojian Chen, Fangfang Li, and Mengxia Liu

Cite this article as:
Jing Wen, Hongyan Sun, Tao Jiang, Bojian Chen, Fangfang Li, and Mengxia Liu, Comparison of the interface reaction behaviors of $CaO–V_2O_5$ and $MnO_2–V_2O_5$ solid-state systems based on the diffusion couple method, *Int. J. Miner. Metall. Mater.*, 30(2023), No. 5, pp. 834-843. https://doi.org/10.1007/s12613-022-2564-7

Articles you may be interested in

Jun-yi Xiang, Xin Wang, Gui-shang Pei, Qing-yun Huang, and Xue-wei Lü, Solid-state reaction of a $CaO–V_2O_5$ mixture: A fundamental study for the vanadium extraction process, *Int. J. Miner. Metall. Mater.*, 28(2021), No. 9, pp. 1462-1468. https://doi.org/10.1007/s12613-020-2136-7

Lei-ying Wang, Li-fan Wang, Rui Wang, Rui Xu, Chun Zhan, Woochul Yang, and Gui-cheng Liu, Solid electrolyte–electrode interface based on buffer therapy in solid-state lithium batteries, *Int. J. Miner. Metall. Mater.*, 28(2021), No. 10, pp. 1584-1602. https://doi.org/10.1007/s12613-021-2278-2

Sheng-chao Duan, Chuang Li, Han-jie Guo, Jing Guo, Shao-wei Han, and Wen-sheng Yang, Investigation of the kinetic mechanism of the demanganization reaction between carbon-saturated liquid iron and CaF_2-CaO-SiO_2-based slags, *Int. J. Miner. Metall. Mater.*, 25(2018), No. 4, pp. 399-404. https://doi.org/10.1007/s12613-018-1584-9

Wang Wei, Hong-rui Yue, and Xiang-xin Xue, Diffusion coefficient of Ti^{4+} in calcium ferrite/calcium titanate diffusion couple, *Int. J. Miner. Metall. Mater.*, 27(2020), No. 9, pp. 1216-1225. https://doi.org/10.1007/s12613-020-2057-5

IJMMM WeChat

QQ author group

International Journal of Minerals, Metallurgy and Materials
Volume 30, Number 5, May 2023, Page 834
https://doi.org/10.1007/s12613-022-2564-7

Comparison of the interface reaction behaviors of $CaO–V_2O_5$ and $MnO_2–V_2O_5$ solid-state systems based on the diffusion couple method

Jing Wen[1)], *Hongyan Sun*[1)], *Tao Jiang*[1,2,3),✉], *Bojian Chen*[1)], *Fangfang Li*[1)], *and Mengxia Liu*[1)]

1) School of Metallurgy, Northeastern University, Shenyang 110819, China
2) Key Laboratory for Ecological Metallurgy of Multimetallic Mineral (Ministry of Education), Northeastern University, Shenyang 110819, China
3) Liaoning Key Laboratory for Metallurgical Sensor and Technology, Shenyang 110819, China
(Received: 12 July 2022; revised: 24 October 2022; accepted: 25 October 2022)

Abstract: The formation mechanism of calcium vanadate and manganese vanadate and the difference between calcium and manganese in the reaction with vanadium are basic issues in the calcification roasting and manganese roasting process with vanadium slag. In this work, $CaO–V_2O_5$ and $MnO_2–V_2O_5$ diffusion couples were prepared and roasted for different time periods to illustrate and compare the diffusion reaction mechanisms. Then, the changes in the diffusion product and diffusion coefficient were investigated and calculated based on scanning electron microscopy (SEM) with energy dispersive X-ray spectroscopy (EDS) analysis. Results show that with the extension of the roasting time, the diffusion reaction gradually proceeds among the $CaO–V_2O_5$ and $MnO_2–V_2O_5$ diffusion couples. The regional boundaries of calcium and vanadium are easily identifiable for the $CaO–V_2O_5$ diffusion couple. Meanwhile, for the $MnO_2–V_2O_5$ diffusion couple, MnO_2 gradually decomposes to form Mn_2O_3, and vanadium diffuses into the interior of Mn_2O_3. Only a part of vanadium combines with manganese to form the diffusion production layer. CaV_2O_6 and MnV_2O_6 are the interfacial reaction products of the $CaO–V_2O_5$ and $MnO_2–V_2O_5$ diffusion couples, respectively, whose thicknesses are 39.85 and 32.13 μm when roasted for 16 h. After 16 h, both diffusion couples reach the reaction equilibrium due to the limitation of diffusion. The diffusion coefficient of the $CaO–V_2O_5$ diffusion couple is higher than that of the $MnO_2–V_2O_5$ diffusion couple for the same roasting time, and the diffusion reaction between vanadium and calcium is easier than that between vanadium and manganese.

Keywords: solid-state reaction; reaction regularity of calcium and vanadium; reaction regularity of manganese and vanadium; diffusion couple method; interface reaction behavior

1. Introduction

Vanadium is an important strategic metal resource in China, which is widely used in the steel chemical industries, aerospace, and other fields due to its excellent physical and chemical properties [1–5]. In particular, in the presence of carbon neutrality and peak carbon dioxide emission targets, the high-tech industry of vanadium, such as vanadium–nitrogen micro-alloyed steel and all-vanadium redox flow battery, is rapidly developing [6–11], which opens up a broad prospect for the development of vanadium products and the utilization of vanadium resources.

Vanadium slag, as the important intermediate product generated during the smelting process of vanadium–titanium magnetite, is the main raw material for vanadium extraction in China [12–15]. Various extraction technologies of vanadium from vanadium slag have been proposed [16–22]. Among them, the calcification roasting process for the treatment of vanadium slag is a hot topic because it effectively avoids many problems in the sodium salt roasting process, such as the generation of harmful gases and hazardous water-soluble vanadium and chromium with high valence state [23–25]. Moreover, a production line with an annual output of 20000 t of V_2O_5 has been established by Xichang Steel and Vanadium Co., Ltd., China, through calcification roasting [26]. In this process, calcium salts, such as $CaCO_3$ and CaO, are used as additives to react with vanadium in vanadium slag to form acid-soluble calcium vanadate, and around 90% of vanadium can be selectively extracted after acid leaching [27]. Furthermore, manganese vanadate and a large number of Mn^{2+} are also detected in roasted materials and a leaching solution, respectively, during the calcification roasting process, which is due to the reaction of vanadium and the original manganese in vanadium slag [28].

Inspired by the calcification roasting process, our group proposed manganese salt roasting, at which $MnCO_3$, MnO_2, and pyrolusite are used as additives to combine with vanadium and generate acid-soluble manganese vanadate [29–31]. This process has higher separation efficiency of vanadium and chromium compared with calcification roasting and avoids the formation of insoluble sulfates. Meanwhile, calcium vanadate is detected in the roasted materials because of the existence of calcium in vanadium slag. Hence, calcium and manganese have strong abilities to combine with va-

✉ Corresponding author: Tao Jiang E-mail: jiangt@smm.neu.edu.cn

nadium. However, there is no systematic study on the formation mechanism of calcium vanadate and manganese vanadate and the difference between calcium and manganese in their interaction with vanadium. These factors have a significant implication for the improvement of basic theory and process optimization during calcification roasting and manganese roasting processes with vanadium slag.

The diffusion couple method is often used to study the mechanism of solid-state reactions. Through observation and analysis of the reaction interface, the phase transition mechanism and product formation in the solid-state reaction, along with the migration rules of essential elements, can be systematically evaluated. For example, Yue *et al.* [32–33] studied the diffusion characteristics of vanadium and calcium in calcium vanadate through V-slag/CaO diffusion. Chen *et al.* [34–35] researched the diffusion behavior between Cr_2O_3 and calcium ferrite based on the diffusion couple method at 1373 K. Ren *et al.* [36] investigated interdiffusion in the Fe_2O_3–TiO_2 system through the diffusion couple method in the temperature range of 1323 to 1473 K. Hence, it is feasible to study and compare the interaction between calcium and manganese when reacting with vanadium through the diffusion couple method.

In this work, V_2O_5 was used to simplify vanadium spinel in vanadium slag to avoid the interference of other impurity elements in vanadium slag. CaO and MnO_2 were used as additives in calcification roasting and manganese roasting, respectively. A CaO–V_2O_5 diffusion couple and MnO_2–V_2O_5 diffusion couple were roasted for different time periods to illustrate and compare the diffusion behavior of the CaO–V_2O_5 and MnO_2–V_2O_5 systems. Furthermore, the diffusion mechanism was studied systematically.

2. Experimental

2.1. Materials

CaO, MnO_2, and V_2O_5 used in this work were all analytical-grade reagents (Sinopharm Chemical Reagent Co., Ltd, China). CaO was roasted at 1000°C for 2 h before use to remove $Ca(OH)_2$ and $CaCO_3$. Fig. 1 presents the X-ray powder diffraction (XRD) patterns of CaO, MnO_2, and V_2O_5. The observed diffraction peaks of the three raw materials are well indexed to those of the Joint Committee on Powder Diffraction Standards, which meet the requirements for the diffusion reaction of the CaO–V_2O_5 and MnO_2–V_2O_5 couples.

2.2. Experimental procedures

2.2.1. Preparation of the diffusion couple

A molded tableting machine was used to press CaO–V_2O_5 and MnO_2–V_2O_5 powders into 8 mm cylinders with two layers. 0.2 g V_2O_5 was first placed into the mold, and 0.2 MPa pressure was applied to ensure a smooth surface of V_2O_5. A drop of ethanol (C_2H_5OH) was dripping on the surface of V_2O_5. Then, 0.2 g CaO or 0.2 g MnO_2 was placed into the mold. After pressing the mold at 2 MPa for 30 s, the CaO–V_2O_5 and MnO_2–V_2O_5 diffusion couples were produced after demolding.

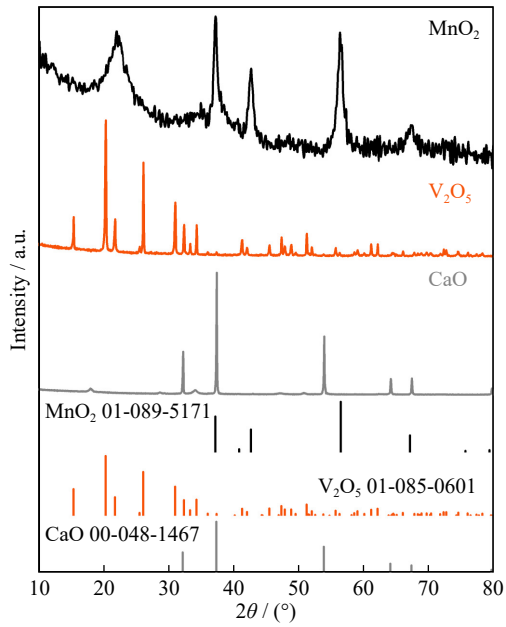

Fig. 1. XRD patterns of CaO, MnO_2, and V_2O_5.

2.2.2. Roasting and diffusion reaction

During the process, the CaO–V_2O_5 and MnO_2–V_2O_5 diffusion couples were placed into a muffle furnace at room temperature and then heated to 600°C at a constant heating rate of 10°C/min. The actual roasting temperature of calcification roasting and manganese salt roasting for vanadium slag was 850–900°C to break down the vanadium-containing spinel structure, realize the oxidation of low-valance vanadium, and promote the formation of acid-soluble vanadate [12,29–30, 37–39]. Meanwhile, analytical-purity V_2O_5 was melted at above 650°C due to its low melting point. Hence, 600°C was chosen as the roasting temperature of the CaO–V_2O_5 and MnO_2–V_2O_5 diffusion couples, which is sufficient for the complete reaction of V_2O_5 with CaO or MnO_2. This conclusion has been confirmed by the powder roasting experiments with three substances in our pre-experiment [40]. During roasting, the diffusion couples were placed into a muffle furnace at room temperature. To investigate the effect of the reaction time on the diffusion reactions of the CaO–V_2O_5 and MnO_2–V_2O_5 systems, the diffusion couples were held at 600°C for 0, 4, 8, 12, 16, and 20 h. After the diffusion reaction, the diffusion couples were taken out and embedded with epoxy resin. The diffusion interface was polished to be observed. Then, the product layer thickness and diffusion coefficient were measured and calculated.

2.3. Characterization

The phases of raw materials were detected using an X-ray diffractometer (X'Pert Pro, PANalytical B.V., Netherlands). Then, a scanning electron microscope (SEM, Ultra plus, Zeiss, Germany) equipped with an energy-dispersive X-ray spectroscope was employed for analyzing the microstructure of diffusion interfaces and the element distribution of vanadium, calcium, and manganese among the roasted CaO–V_2O_5 and MnO_2–V_2O_5 diffusion couples. The experimental process of this work is shown in Fig. 2.

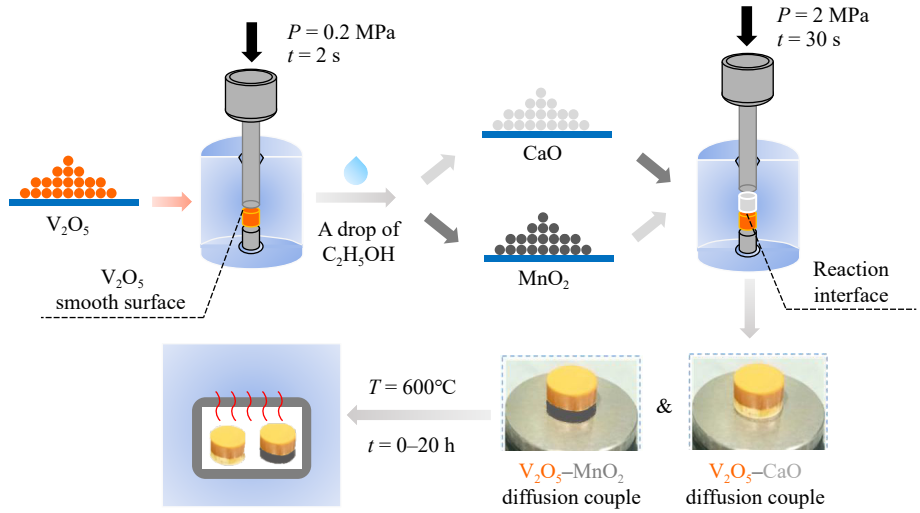

Fig. 2. Experimental process of this work. *P*—Pressure; *t*—Time; *T*—Temperature.

3. Results and discussion

3.1. Morphology of the diffusion couples

Fig. 3 shows the SEM images and element distribution of the CaO–V_2O_5 and MnO_2–V_2O_5 diffusion couples holding at 600°C for 0 h. The micrographs with different magnifications show that the particles on the right side are denser than those on the left side in the CaO–V_2O_5 couple, as shown in Fig. 3(a) and (b). Combined with the distribution of calcium and vanadium elements in Fig. 3(c) and (d), CaO and V_2O_5 are on the left and right sides in the field of vision, respectively. Furthermore, according to the EDS analysis of points A and B in Fig. 3(e) and (f), the two sides of the diffusion couple are still CaO and V_2O_5 after raising the temperature to 600°C and holding for 0 h.

In Fig. 3(g)–(l), similar phenomena occur in the MnO_2–V_2O_5 diffusion couple. The phase containing vanadium on the right side of the diffusion couple is denser than that containing manganese on the left side, as shown in Fig. 3(g)–(j). Meanwhile, as shown in Fig. 3(k), the atomic ratio of oxygen to manganese at point C is 1.45, which is closer to the atomic ratio of oxygen to manganese in Mn_2O_3 of 1.5, rather than the value of MnO_2 of 2. Hence, MnO_2 has been decomposed into Mn_2O_3 after roasting from room temperature to 600°C. The reaction equation is shown in Eq. (1):

$$4MnO_2 = 2Mn_2O_3 + O_2(g) \quad (1)$$

This conclusion has also been further verified by the XRD results. Mn_2O_3 and V_2O_5 are on the left and right sides, respectively. Moreover, no obvious product layer can be observed on the interface of the CaO–V_2O_5 and MnO_2–V_2O_5 diffusion couples without keeping at 600°C for a period of time. There is also no coincidence of the element distribu-

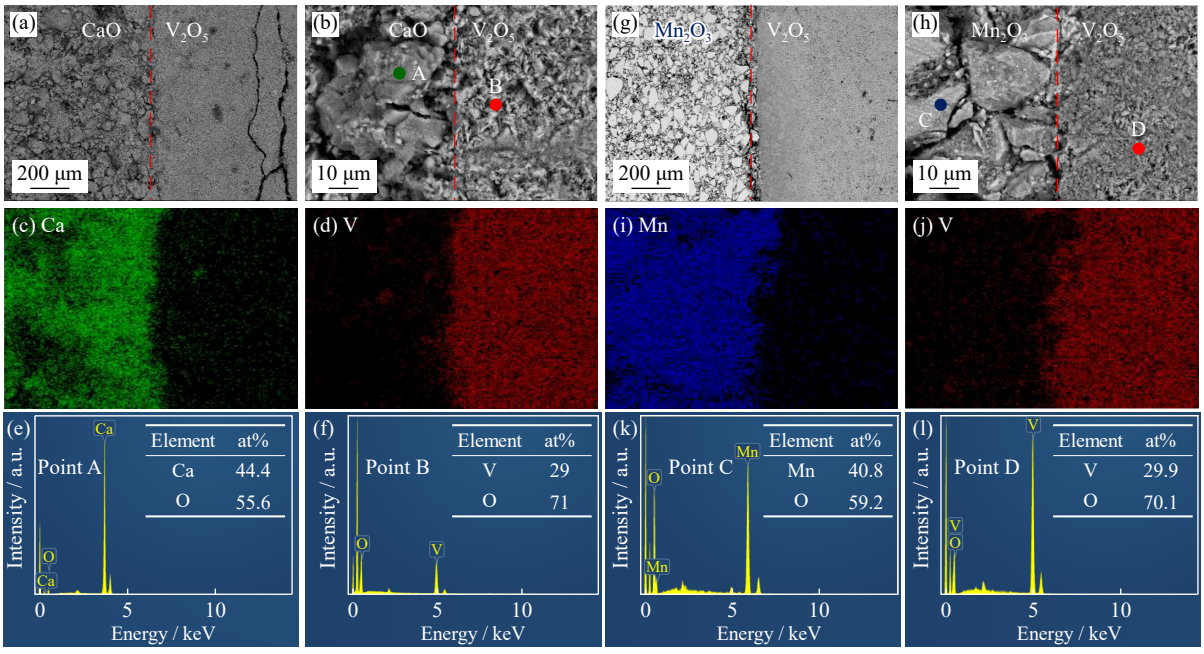

Fig. 3. (a, b) SEM images of the CaO–V_2O_5 diffusion couple at 600°C for 0 h; (c, d) element mapping of (b); (e, f) EDS analysis of points A and B in (b). (g, h) SEM images of the MnO_2–V_2O_5 diffusion couple at 600°C for 0 h; (i, j) element mapping of (h); (k, l) EDS analysis of points C and D in (h).

tions of vanadium and calcium, along with vanadium and manganese, confirming that diffusion reactions did not take place among the $CaO–V_2O_5$ and $MnO_2–V_2O_5$ couples.

Figs. 4 and 5 show the changes in the micromorphology of the $CaO–V_2O_5$ and $MnO_2–V_2O_5$ diffusion couples under the same magnification after roasting at 600°C for different time periods, respectively. In Fig. 4, the diffusion interface of the $CaO–V_2O_5$ diffusion couple is clear. Moreover, the diffusion product in the center of the visual field can easily be identified, whose grayscale is notably different from that of CaO and V_2O_5. Moreover, the product layer is denser than CaO and V_2O_5. The thickness of the product layer gradually increases with the extension of the roasting time, which does not significantly increase after 16 h.

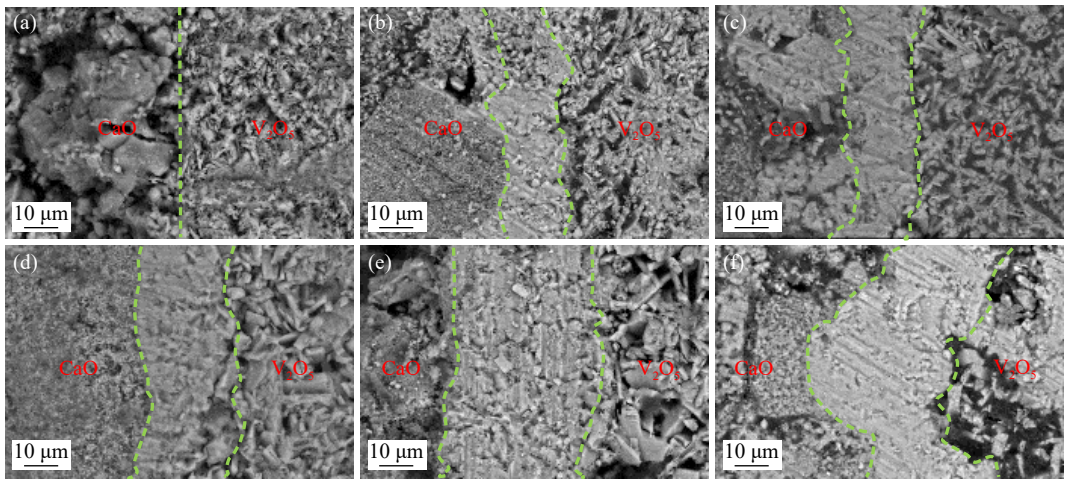

Fig. 4. SEM images of the $CaO–V_2O_5$ diffusion couples after roasting at 600°C for different time periods: (a) 0 h; (b) 4 h; (c) 8 h; (d) 12 h; (e) 16 h; (f) 20 h.

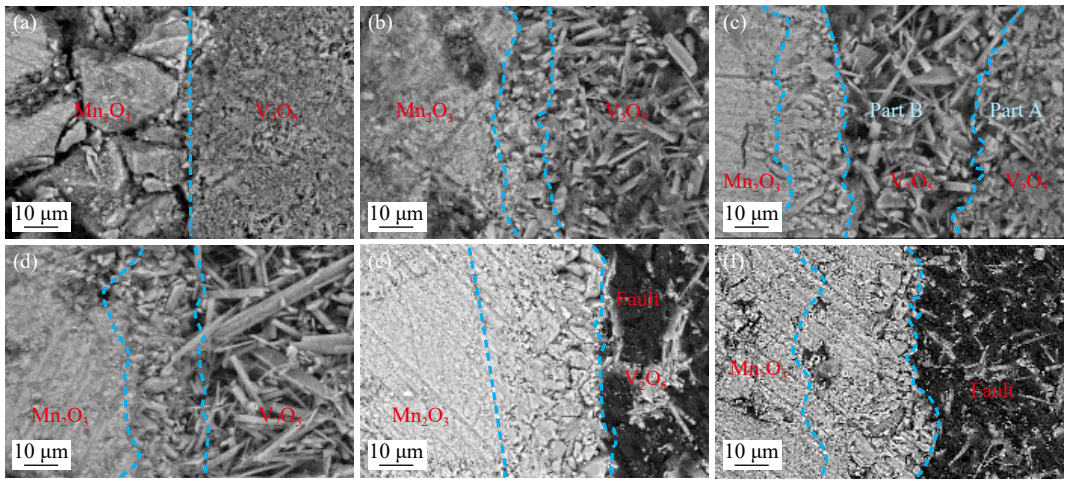

Fig. 5. SEM images of the $MnO_2–V_2O_5$ diffusion couples after roasting at 600°C for different time periods: (a) 0 h; (b) 4 h; (c) 8 h; (d) 12 h; (e) 16 h; (f) 20 h.

For the $MnO_2–V_2O_5$ diffusion couple in Fig. 5, in the diffusion reaction progress of manganese oxide and V_2O_5, the micromorphology of V_2O_5 greatly changes. At 0 h, V_2O_5 is shown as small particles. With the extension of the roasting time, V_2O_5 particles are like slender needle-like dendrites, and the gap between V_2O_5 particles at the interface is large. This phenomenon is further reflected intuitively in the diffusion couple after roasting for 8 h. V_2O_5 with the above two morphologies are reflected in parts A and B, respectively. When the roasting time exceeds 16 h, there is no V_2O_5 layer in the field of vision, but it is replaced by a wide fault zone.

To further investigate the difference between calcium and manganese in the diffusion reaction process with vanadium, the $CaO–V_2O_5$ and $MnO_2–V_2O_5$ diffusion couples roasted for 16 h are compared in detail. The results show that after the roasting process, the thickness of the product layers does not increase obviously. The morphology and element distribution at the interface of the $CaO–V_2O_5$ diffusion couple after roasting the $CaO–V_2O_5$ and $MnO_2–V_2O_5$ diffusion couples at 600°C for 16 h are shown in Fig. 6. In Fig. 6(a) and (b), the diffusion product of CaO and V_2O_5 in the center of the visual field is obvious, and the product layer is denser than those of CaO and V_2O_5. According to the element mapping of Fig. 6(c) and (d), the distribution regions of vanadium and calcium are partly coincident, which is due to the diffusion reaction of CaO and V_2O_5 and the formation of calcium vanadate. Based on the line-scan analysis of calcium and vanadium in Fig. 6(e), the distribution of calcium and vana-

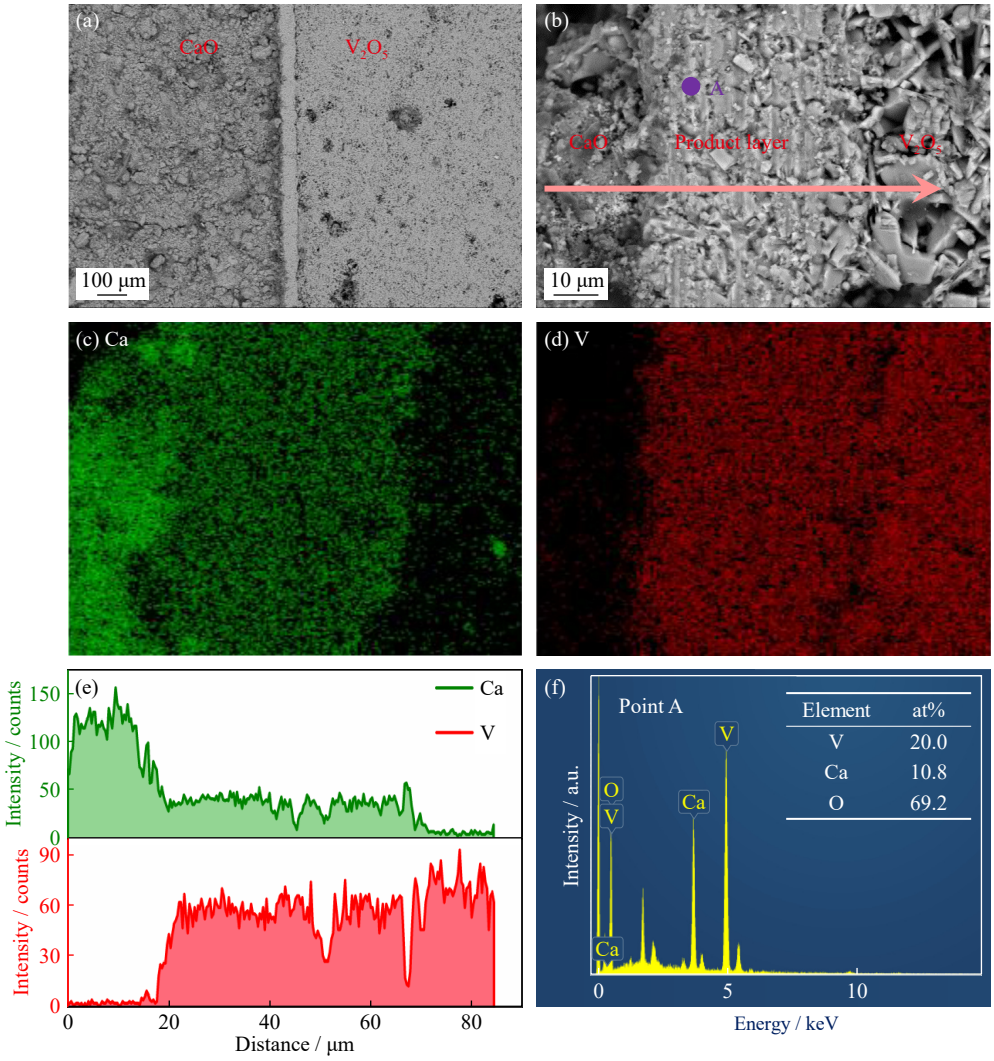

Fig. 6. SEM images and corresponding EDS results the $CaO–V_2O_5$ diffusion couple roasted at 600°C for 16 h: (a, b) morphologies with different magnifications; (c, d) element mapping images of (b); (e) line-scan analysis; (f) EDS analysis of point A).

dium shows a three-stage change. On the CaO side, the content of calcium reaches a high level, but there is no vanadium. In the diffusion product layer, the content of vanadium significantly increases with the reaction between CaO and V_2O_5, and the content of calcium decreases due to the formation of reaction products, as shown in Fig. 6(e). On the V_2O_5 side, calcium cannot be easily detected, whereas the content of vanadium reaches a high level. The EDS analysis in Fig. 6(f) shows that the atomic ratio of vanadium and calcium is 1.85, and the atomic ratio of oxygen and calcium is 6.41, close to the values of CaV_2O_6. Hence, the diffusion-layer product is supposed to be calcium metavanadate (CaV_2O_6).

Fig. 7 shows the morphology and element distribution at the interface of the $MnO_2–V_2O_5$ diffusion couple after roasting for 16 h. MnO_2 on the left side of the $MnO_2–V_2O_5$ diffusion couple is further decomposed into Mn_2O_3. As shown in Fig. 7(a), the whole visual field can be divided into five parts. Combined with the element mapping and line-scan analysis in Fig. 7(b)–(d), part I is V_2O_5. With the gradual diffusion of V_2O_5 to Mn_2O_3, a fault exists in the V_2O_5 side, as shown in part II, which is attributed to the fact that the diffusion ability of vanadium to the product layer and the Mn_2O_3 side is far stronger than that of manganese to the product layer and V_2O_5. This condition results in the gradual diffusion of vanadium near the diffusion couple interface into Mn_2O_3. Moreover, an obvious fault zone appears on the V_2O_5 side away from the diffusion couple interface. After the fault zone, a dense area including part III and part IV appears on the Mn_2O_3 side. Due to many pores in the Mn_2O_3 side, vanadium is easily diffused and entered the inside of Mn_2O_3. Meanwhile, only part of the vanadium can combine with manganese to form manganese vanadate and form the diffusion production layer, as shown in part III. Hence, the existence of pores in the Mn_2O_3 side makes the diffusion of vanadium easy and accelerates the diffusion reaction of vanadium and manganese. In part IV, although vanadium has diffused into the Mn_2O_3 side, it only fills the pores on the manganese side. The low concentrations of vanadium and manganese make the kinetic conditions of their reaction poor and make it difficult for them to continue the reaction and form the product layer. Moreover, almost no vanadium is detected, indicating that part V is Mn_2O_3.

The diffusion reaction between V_2O_5 and Mn_2O_3 is further verified, as shown in Fig. 7(e)–(g). A clear fault zone is ob-

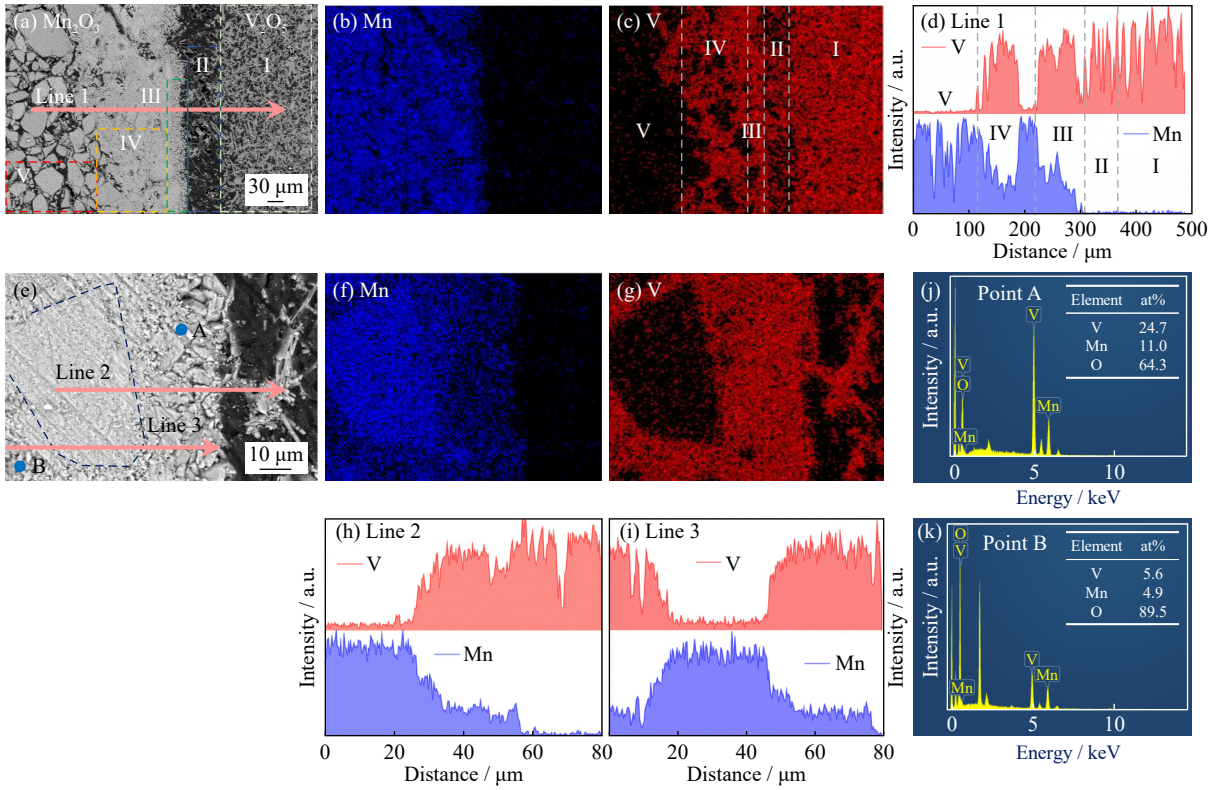

Fig. 7. SEM images and corresponding EDS results of the $MnO_2–V_2O_5$ diffusion couple roasted at 600°C for 16 h: (a, e) morphology with different magnifications; (b, c) element mapping images of (a); (d) line-scan analysis of line 1 in (a); (f, g) element mapping images of (e); (h, i): line-scan analysis of lines 2 and 3 in (e); (j, k) EDS analysis of points A and B.

served due to differences in the diffusion ability of vanadium and manganese. Only manganese is detected in the area surrounded by the dotted line, which is considered to be Mn_2O_3. In the area around Mn_2O_3, vanadium and manganese simultaneously exist. Meanwhile, the EDS results show that points A and B are not the same substance. Point A is located inside the diffusion product layer of vanadium and manganese, where the atomic ratio of vanadium to manganese is close to 2, and the atomic ratio of oxygen to manganese is close to 6. The value is close to the values of manganese metavanadate MnV_2O_6. Hence, the diffusion-layer product is supposed to be MnV_2O_6. Point B is located inside Mn_2O_3, where the atomic ratio of vanadium to manganese is not like that in the product layer. Point B is the simple diffusion of vanadium into the gap of Mn_2O_3. The above studies show obvious differences in the reaction between CaO and Mn_2O_3 with V_2O_5.

Fig. 8 shows the atomic ratios of vanadium to calcium or vanadium to manganese in the product layers when the $CaO–V_2O_5$ and $MnO_2–V_2O_5$ diffusion couples are roasted at 600°C for different time periods. In Fig. 8(a), the atomic ratios of vanadium to calcium in the product layers are approximately 2 under different roasting times, which indicates that the diffusion product of the $CaO–V_2O_5$ couples is CaV_2O_6. The atomic ratios of vanadium to manganese in the product layer shown in Fig. 8(b) are also approximately 2 when the roasting time ranges from 0 to 20 h. Hence, MnV_2O_6 is sup-

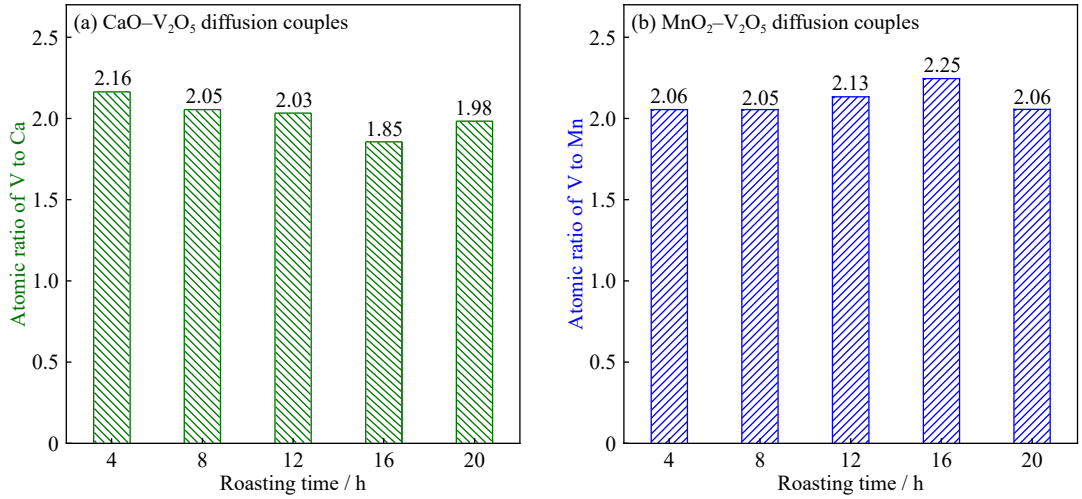

Fig. 8. Effect of the roasting time on the diffusion products of the $CaO–V_2O_5$ and $MnO_2–V_2O_5$ couples.

posed to be the diffusion product of the MnO_2–V_2O_5 couples. These results show that the diffusion reaction products are stable and do not change with the extension of the reaction time.

3.2. Calculation of the product layer thickness and diffusion coefficient

When the roasting temperature is kept at 600°C, the diffusion reactions gradually proceed among the CaO–V_2O_5 and MnO_2–V_2O_5 diffusion couples with the extension of the roasting time, and the thicknesses of the product layers increase. Based on the micromorphology and line scanning results of the CaO–V_2O_5 diffusion couples at different roasting times, the image of the product layers is supposed to be divided into 24 regions at an equal distance (ΔH) along the vertical direction of the sample cross section. The diffusion-layer thicknesses between L_1 to L_{25} are measured according to the image scale. Then, the average value L is taken according to Eq. (2), which is considered to be the thickness of the diffusion layers of the CaO–V_2O_5 diffusion couples [36,41].

$$L = \frac{L_1 + L_2 + \ldots + L_{25}}{25} \tag{2}$$

The diffusion-layer thicknesses of the MnO_2–V_2O_5 diffusion couples at different roasting times are also measured and calculated by this method. The results of the product layer thickness are shown in Fig. 9.

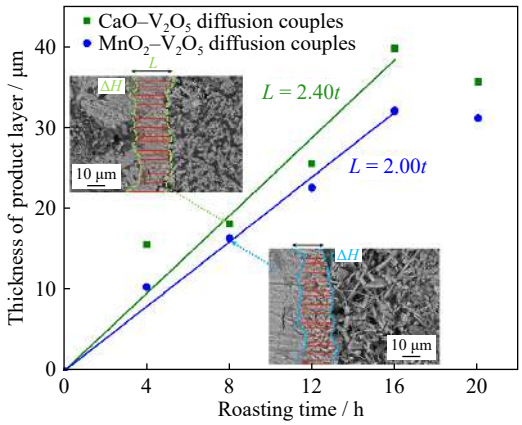

Fig. 9. Relationships between the product layer thickness and roasting time of two diffusion couples.

The results show that the thicknesses of the product layer (L) increase with the extension of the roasting time, which remarkably increase from 0 to 16 h and remain stable after 20 h among the CaO–V_2O_5 and MnO_2–V_2O_5 diffusion couples. The L values of the CaO–V_2O_5 and MnO_2–V_2O_5 diffusion couples are 39.85 and 32.13 μm at 16 h, respectively. Accordingly, the relationships between the product layer thickness and roasting time of the two diffusion couples are fitted at 0–16 h, as shown in Eqs. (3) and (4).

CaO–V_2O_5 diffusion couple:

$$L = 2.40t \tag{3}$$

MnO_2–V_2O_5 diffusion couple:

$$L = 2.00t \tag{4}$$

where L is the thickness of the product layer of the two diffusion couples, μm, and t is the roasting time of diffusion reaction, h. The relationships between the diffusion-layer thickness and roasting time are basically linear at 0–16 h, as shown in Fig. 9. The determination coefficient R^2 values of the CaO–V_2O_5 and MnO_2–V_2O_5 diffusion couples are both 0.99, which illustrates that the fitting equations are suited for describing the relationships between the product layer thickness and roasting time. The reaction coefficient of the CaO–V_2O_5 diffusion couple is 2.40, which is higher than that of the MnO_2–V_2O_5 diffusion couple (2.00). This finding confirms that the reaction between vanadium and calcium is easier than that between vanadium and manganese at the same roasting temperature and roasting time.

Furthermore, the activation of the diffusion reaction of CaO and V_2O_5 or MnO_2 and V_2O_5 is expected to be constant due to the linear relationship between the product layer thickness and roasting time. Then, the diffusion coefficients D of the CaO–V_2O_5 and MnO_2–V_2O_5 diffusion couples can be calculated by Eq. (5) [34,42], as shown in Fig. 10.

$$L^2 = 4Dt \tag{5}$$

The results show that with the extension of the roasting time, the diffusion coefficients (D) basically increase first and then decrease among the CaO–V_2O_5 and MnO_2–V_2O_5 diffusion couples. The maximum values are achieved at 16 h, which are 6.89×10^{-11} and 4.48×10^{-11} $cm^2 \cdot s^{-1}$. Hence, prolonging the roasting time is beneficial to the diffusion reactions of the CaO–V_2O_5 and MnO_2–V_2O_5 diffusion couples. After 16 h, the diffusion reactions reach the equilibrium states on the whole, and the diffusion coefficients decrease. Furthermore, the diffusion coefficient D of the CaO–V_2O_5 diffusion couple is higher than that of the MnO_2–V_2O_5 diffusion couple at the same roasting time, which further confirms that calcium is slightly stronger than manganese in terms of the reaction ability with vanadium.

3.3. Diffusion mechanism of the diffusion couples

Based on the above analyses, the diffusion reaction mechanisms of the CaO–V_2O_5 and MnO_2–V_2O_5 diffusion couples are summarized in Fig. 11. For the CaO–V_2O_5 diffusion couple, the diffusion ability of vanadium to the product layer

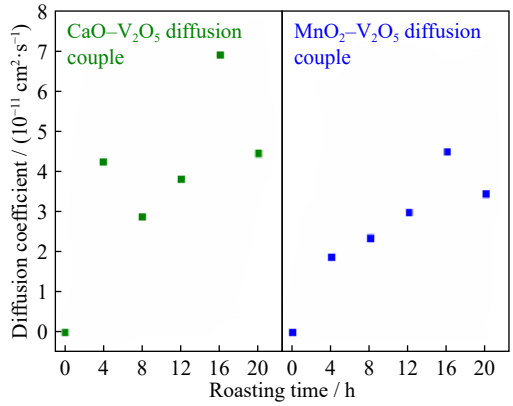

Fig. 10. Relationships between the diffusion coefficient and roasting time of CaO–V_2O_5 and MnO_2–V_2O_5 diffusion couples.

and CaO side is close to that of calcium to the product layer and V_2O_5 side. With the extension of the roasting time, vanadium and calcium continue to contact and react to form CaV_2O_6, and their thicknesses gradually increase. After roasting for 16 h, it is difficult for vanadium or calcium molecules to pass through the product layer, which may be related to the molecular diffusion ability of vanadium and calcium or the thickness and density of the product layer. Thus, vanadium and calcium cannot easily contact each other, and the diffusion reaction would not be continued.

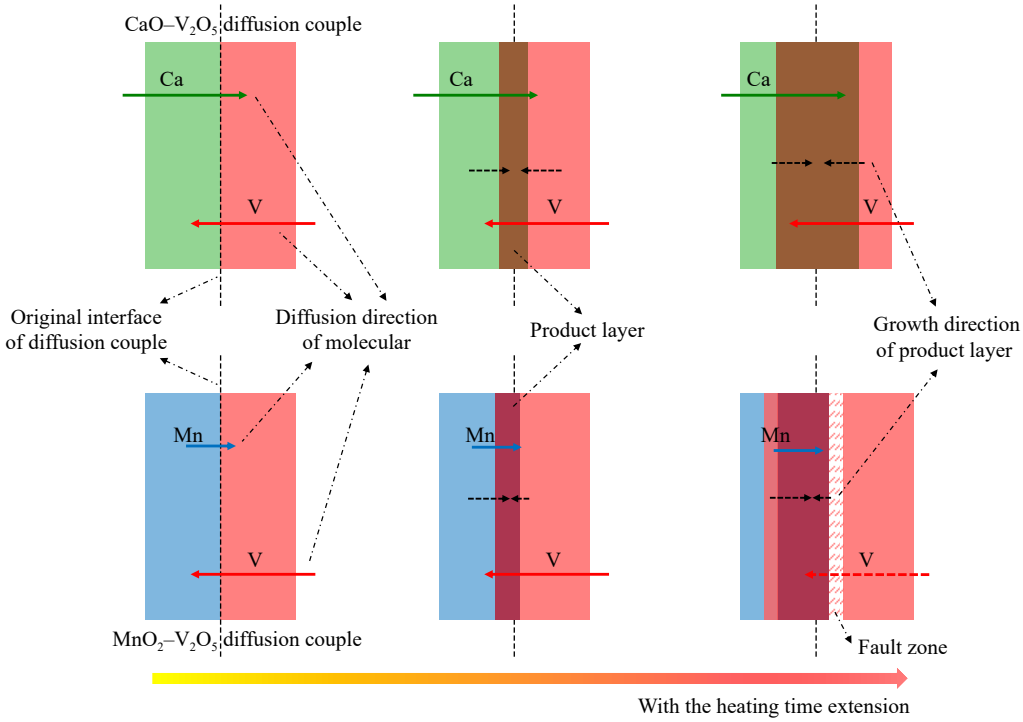

Fig. 11. Diffusion reaction mechanisms of the $CaO–V_2O_5$ and $MnO_2–V_2O_5$ diffusion couples.

For the $MnO_2–V_2O_5$ diffusion couple, the diffusion ability of vanadium to the product layer and Mn_2O_3 side is far stronger than that of manganese to the product layer and V_2O_5. With the extension of the roasting time, the diffusion-layer thickness increases mainly due to the reaction between vanadium and manganese on the Mn_2O_3 side. Even when the roasting time reaches 16 h, an obvious fault zone appears on the V_2O_5 side away from the diffusion couple interface. At this time, vanadium diffuses into the Mn_2O_3 side has reached the reaction equilibrium with manganese, whereas vanadium on the V_2O_5 side cannot easily diffuse to the Mn_2O_3 side and break the reaction equilibrium due to the existence of the fault zone. Therefore, the thickness of the product layer no longer increases after 16 h.

4. Conclusions

In this work, the reaction mechanism of calcium and manganese in the reaction with vanadium was investigated and compared through the diffusion couple method. V_2O_5 was used to simulate and simplify vanadium slag to avoid the interference of other impurity elements. The $CaO–V_2O_5$ and $MnO_2–V_2O_5$ diffusion couples were roasted for different time periods to illustrate the diffusion interface, diffusion products, and diffusion coefficient of the $CaO–V_2O_5$ and $MnO_2–V_2O_5$ systems. Accordingly, the following conclusions can be drawn.

(1) During the diffusion reaction of the $CaO–V_2O_5$ couple, calcium and vanadium always exist in the form of CaO and V_2O_5. The product layer and boundaries of calcium and vanadium are obvious. For the $MnO_2–V_2O_5$ couple, MnO_2 is gradually decomposed into Mn_2O_3. Vanadium can diffuse into the interior of manganese, whereas only part of vanadium combines with manganese to form the diffusion production layer. The particles of V_2O_5 are stretched, and a fault even appears in the V_2O_5 side with the extension of the diffusion time, which is attributed to the fact that the diffusion ability of vanadium to the product layer and Mn_2O_3 side is far stronger than that of manganese to the product layer and V_2O_5.

(2) The atomic ratios of calcium to vanadium or manganese to vanadium in the product layers of the $CaO–V_2O_5$ and $MnO_2–V_2O_5$ diffusion couples are approximately 2 for different roasting times, confirming that the diffusion products of the $CaO–V_2O_5$ and $MnO_2–V_2O_5$ diffusion couples are CaV_2O_6 and MnV_2O_6, respectively.

(3) The thickness of the product layer gradually increases with the extension of the roasting time, which does not significantly increase after 16 h. The diffusion product layer thickness of the $CaO–V_2O_5$ and $MnO_2–V_2O_5$ diffusion couples are 39.85 and 32.13 μm at 16 h. After 16 h, the two diffusion couples reach the reaction equilibrium due to the limitation of diffusion. Moreover, the diffusion coefficient of the $CaO–V_2O_5$ diffusion couple is higher than that of the $MnO_2–V_2O_5$

diffusion couple at the same roasting time. Hence, the diffusion reaction between vanadium and calcium is easier than that between vanadium and manganese.

Acknowledgements

This work was financially supported by the National Natural Science Foundation of China (Nos. 52174277 and 51874077), the Fundamental Funds for the Central Universities, China (No. N2225032), the China Postdoctoral Science Foundation (No. 2022M720683), and the Postdoctoral Fund of Northeastern University, China.

Conflict of Interest

The authors have no relevant financial or non-financial interests to disclose.

References

[1] R.R. Moskalyk and A.M. Alfantazi, Processing of vanadium: A review, *Miner. Eng.*, 16(2003), No. 9, p. 793.
[2] X.M. Xu, F.Y. Xiong, J.S. Meng, *et al*., Vanadium-based nanomaterials: A promising family for emerging metal-ion batteries, *Adv. Funct. Mater.*, 30(2020), No. 10, art. No. 1904398.
[3] P.W. Shen, Y.X. Che, H.J. Luo, and Y.D. Gu, *Inorganic Chemistry Books*, Science Press, Beijing, 2008.
[4] S.Z. Yang, *Vanadium Metallurgy*, Metallurgical Industry Press, Beijing, 2010.
[5] Y.M. Zhang, S.X. Bao, T. Liu, T.J. Chen, and J. Huang, The technology of extracting vanadium from stone coal in China: History, current status and future prospects, *Hydrometallurgy*, 109(2011), No. 1-2, p. 116.
[6] Y.N. Fan, F. Ma, J.S. Liang, *et al*., Accelerated polysulfide conversion on hierarchical porous vanadium–nitrogen–carbon for advanced lithium-sulfur batteries, *Nanoscale*, 12(2020), No. 2, p. 584.
[7] J.M. Zhu, P. Zhao, M.H. Jing, H.J. Wu, and J.J. Li, Preparation of vanadium–nitrogen alloy at low temperature by a coupled electric and thermal field, *Vacuum*, 195(2022), art. No. 110644.
[8] Y. Shi, C.K. Eze, B.Y. Xiong, *et al*., Recent development of membrane for vanadium redox flow battery applications: A review, *Appl. Energy*, 238(2019), p. 202.
[9] Y.Q. Jiang, M.C. Du, G. Cheng, *et al*., Nanostructured N-doped carbon materials derived from expandable biomass with superior electrocatalytic performance towards V^{2+}/V^{3+} redox reaction for vanadium redox flow battery, *J. Energy Chem.*, 59(2021), p. 706.
[10] K. Lourenssen, J. Williams, F. Ahmadpour, R. Clemmer, and S. Tasnim, Vanadium redox flow batteries: A comprehensive review, *J. Energy Storage*, 25(2019), art. No. 100844.
[11] Y.R. Lv, C. Han, Y. Zhu, *et al*., Recent advances in metals and metal oxides as catalysts for vanadium redox flow battery: Properties, structures, and perspectives, *J. Mater. Sci. Technol.*, 75(2021), p. 96.
[12] J.Y. Xiang, Q.Y. Huang, X.W. Lv, and C.G. Bai, Multistage utilization process for the gradient-recovery of V, Fe, and Ti from vanadium-bearing converter slag, *J. Hazard. Mater.*, 336(2017), p. 1.
[13] M. Li, S.L. Zheng, B. Liu, *et al*., A clean and efficient method for recovery of vanadium from vanadium slag: Nonsalt roasting and ammonium carbonate leaching processes, *Miner. Process. Extr. Metall. Rev.*, 38(2017), No. 4, p. 228.
[14] H.Y. Gao, T. Jiang, Y.Z. Xu, J. Wen, and X.X. Xue, Change in phase, microstructure, and physical-chemistry properties of high chromium vanadium slag during microwave calcification-roasting process, *Powder Technol.*, 340(2018), p. 520.
[15] Z.H. Dong, J. Zhang, and B.J. Yan, A new approach for the comprehensive utilization of vanadium slag, *Metall. Mater. Trans. B*, 53(2022), No. 4, p. 2198.
[16] Y. Guo, H.Y. Li, Y.H. Yuan, *et al*., Microemulsion leaching of vanadium from sodium-roasted vanadium slag by fusion of leaching and extraction processes, *Int. J. Miner. Metall. Mater.*, 28(2021), No. 6, p. 974.
[17] J.C. Lee, Kurniawan, E.Y. Kim, K.W. Chung, R. Kim, and H.S. Jeon, A review on the metallurgical recycling of vanadium from slags: Towards a sustainable vanadium production, *J. Mater. Res. Technol.*, 12(2021), p. 343.
[18] H.Y. Li, C.J. Wang, M.M. Lin, Y. Guo, and B. Xie, Green one-step roasting method for efficient extraction of vanadium and chromium from vanadium–chromium slag, *Powder Technol.*, 360(2020), p. 503.
[19] Y. Guo, H.Y. Li, S. Shen, C.J. Wang, J. Diao, and B. Xie, Recovery of vanadium from vanadium slag with high phosphorus content via recyclable microemulsion extraction, *Hydrometallurgy*, 198(2020), art. No. 105509.
[20] J.Y. Xiang, X. Wang, G.S. Pei, Q.Y. Huang, and X.W. Lü, Solid-state reaction of a $CaO–V_2O_5$ mixture: A fundamental study for the vanadium extraction process, *Int. J. Miner. Metall. Mater.*, 28(2021), No. 9, p. 1462.
[21] M. Li, B. Liu, S.L. Zheng, *et al*., A cleaner vanadium extraction method featuring non-salt roasting and ammonium bicarbonate leaching, *J. Cleaner Prod.*, 149(2017), p. 206.
[22] S.Y. Liu, X.B. He, Y.D. Wang, and L.J. Wang, Cleaner and effective extraction and separation of iron from vanadium slag by carbothermic reduction–chlorination–molten salt electrolysis, *J. Cleaner Prod.*, 284(2021), art. No. 124674.
[23] P. Cao, Research on vanadium slag roasted with calcium salt, *Iron Steel Vanadium Titanium*, 33(2012), No. 1, p. 30.
[24] J.Y. Xiang, Q.Y. Huang, X.W. Lv, and C.G. Bai, Extraction of vanadium from converter slag by two-step sulfuric acid leaching process, *J. Cleaner Prod.*, 170(2018), p. 1089.
[25] J. Wen, T. Jiang, Y.Z. Xu, J. Cao, and X.X. Xue, Efficient extraction and separation of vanadium and chromium in high chromium vanadium slag by sodium salt roasting–$(NH_4)_2SO_4$ leaching, *J. Ind. Eng. Chem.*, 71(2019), p. 327.
[26] *Brief Introduction of Xichang Steel Vanadium Co., Ltd. of Panzhihua Iron and Steel Group* [2022-06-30], https://www.pzhsteel.com.cn/xcgf/ind ex.php?s=/Home/Article/pg_jianjie/art_bm_id/89/fl/two/msg_id/156.
[27] J. Wen, T. Jiang, M. Zhou, H.Y. Gao, J.Y. Liu, and X.X. Xue, Roasting and leaching behaviors of vanadium and chromium in calcification roasting–acid leaching of high-chromium vanadium slag, *Int. J. Miner. Metall. Mater.*, 25(2018), No. 5, p. 515.
[28] T.X. Yu, T. Jiang, J. Wen, H.Y. Sun, M. Li, and Y. Peng, Effect of chemical composition on the element distribution, phase composition and calcification roasting process of vanadium slag, *Int. J. Miner. Metall. Mater.*, 29(2022), No. 12, p. 2144.
[29] J. Wen, T. Jiang, H.Y. Sun, and T.X. Yu, Novel understanding of simultaneous extraction of vanadium and manganese from vanadium slag and low-grade pyrolusite based on selective oxidation–reduction roasting, *ACS Sustainable Chem. Eng.*, 8(2020), No. 15, p. 5927.
[30] J. Wen, T. Jiang, J.P. Wang, H.Y. Gao, and L.G. Lu, An efficient utilization of high chromium vanadium slag: Extraction of vanadium based on manganese carbonate roasting and detoxification processing of chromium-containing tailings, *J. Hazard. Mater.*, 378(2019), art. No. 120733.
[31] J. Wen, T. Jiang, J.P. Wang, L.G. Lu, and H.Y. Sun, Cleaner

extraction of vanadium from vanadium-chromium slag based on MnO_2 roasting and manganese recycle, *J. Cleaner Prod.*, 261(2020), art. No. 121205.

[32] H.R. Yue and X.X. Xue, Generated compounds at the V-slag/CaO diffusion surface and diffusion characteristics of V and Ca in calcium vanadate, *J. Hazard. Mater.*, 393(2020), art. No. 122368.

[33] H.R. Yue and X.X. Xue, Evolution of generated calcium vanadates at different locations in the vicinity of the V_2O_5/CaO interface with annealing parameters, *Metall. Mater. Trans. B*, 51(2020), No. 5, p. 2358.

[34] B.J. Chen, M. Zhou, T. Jiang, and L. Li, Observation of diffusion behavior between Cr_2O_3 and calcium ferrite based on diffusion couple method at 1373 K, *J. Alloys Compd.*, 802(2019), p. 103.

[35] B.J. Chen, T. Jiang, M. Zhou, L. Li, J. Wen, and Y.C. Wen, Interdiffusion kinetics and solid-state reaction mechanism between Cr_2O_3 and calcium ferrite based on diffusion couple method, *J. Alloys Compd.*, 865(2021), art. No. 158754.

[36] Z.S. Ren, X.J. Hu, X.X. Xue, and K. Chou, Solid state reaction studies in Fe_3O_4–TiO_2 system by diffusion couple method, *J. Alloys Compd.*, 580(2013), p. 182.

[37] J.H. Zhang, W. Zhang, L. Zhang, and S.Q. Gu, Mechanism of vanadium slag roasting with calcium oxide, *Int. J. Miner. Process.*, 138(2015), p. 20.

[38] J.H. Zhang, W. Zhang, and Z.L. Xue, Oxidation kinetics of vanadium slag roasting in the presence of calcium oxide, *Miner. Process. Extr. Metall. Rev.*, 38(2017), No. 5, p. 265.

[39] J. Wen, T. Jiang, X.L. Zheng, J.P. Wang, J. Cao, and M. Zhou, Efficient separation of chromium and vanadium by calcification roasting–sodium carbonate leaching from high chromium vanadium slag and V_2O_5 preparation, *Sep. Purif. Technol.*, 230(2020), art. No. 115881.

[40] H.Y. Sun, *Study on Formation Mechanism of Calcium Vanadate/Chromate during Calcification Roasting Process of High-chromium Vanadium Slag* [Dissertation], Northeastern University, Shenyang, 2021.

[41] M.F. Jin, G.S. Li, M.S. Chu, and F.M. Shen, Diffusion between MgO and hematite during sintering, *Iron Steel*, 43(2008), No. 3, p. 10.

[42] H.Y. Sun, J. Wen, B.J. Chen, T.X. Yu, and T. Jiang, Solid phase reaction and diffusion behavior of V_2O_5/Cr_2O_3–CaO system based on calcification roasting of chromium-containing vanadium slag, *Iron Steel Vanadium Titanium*, 42(2021), No. 3, p. 17.